

**Spatially-Resolved Lunar Phase Function at 1064 nm from Lunar Orbiter Laser Altimeter (LOLA) Passive Radiometry.** R. T. Walker<sup>1,2</sup>, M. K. Barker<sup>1</sup>, X. Sun<sup>1</sup>, E. Mazarico<sup>1</sup>, D. E. Smith<sup>3</sup>, M. T. Zuber<sup>3</sup> and G. A. Neumann<sup>1</sup>. <sup>1</sup>Solar System Exploration Division, NASA Goddard Space Flight Center, 8800 Greenbelt Rd., Greenbelt, MD 20771 (ryan.t.walker@nasa.gov), <sup>2</sup>Hexagon US Federal, 4600 Forbes Blvd, Lanham, MD 20706, <sup>3</sup>Dept. of Earth, Atmospheric and Planetary Sciences, MIT, 77 Massachusetts Ave., Cambridge, MA 02139.

**Introduction:** The reflectance of the lunar surface is a function of wavelength, viewing/illumination geometry, the scattering behavior of the regolith particles, and the micro-texture of the surface. These properties hold vital clues to many surface processes operating on airless bodies throughout the solar system. Therefore, it is crucial to fully characterize the surface reflectance over as wide a range in wavelengths and geometries as possible. To that end, the Lunar Orbiter Laser Altimeter (LOLA) onboard the Lunar Reconnaissance Orbiter (LRO) has been making photometric measurements of the lunar surface for over 8 years. When not in altimetry mode, LOLA's laser is turned off and it acts as a near-infrared ( $1064 \pm 0.2$  nm) passive radiometer. In this mode, the threshold and gain of the detectors are adjusted such that the solar photons reflected off the lunar surface that are “noise” for altimetry are actually the signal. LOLA collects raw passive radiometry data at a rate of 28 Hz over a footprint of  $\sim 120$  m from a 100 km altitude. We show results for data collected from December 2013 through December 2021, over 3.8 billion observations with nearly pole-to-pole coverage.

**Calibration:** Even without incident light, thermal electrons in the detectors (“dark current”) cause nonzero counts. We fit these raw nighttime noise counts with a cubic function of time and detector temperature and subtract the result from the raw daytime counts. We convert the dark-subtracted LOLA counts to absolute radiance by referencing against JAXA's SELENE (Kaguya) Multiband Imager Mosaic [1] and Spectral Profiler photometric function [2]. These yield the radiance factor (RADF, or I/F) at the actual geometry of each LOLA observation. We then fit the ratio of RADF/counts with a quadratic function of time and detector temperature. Each channel is calibrated separately, and then all channels are averaged to improve signal-to-noise [3].

**Photometry:** Topography-dependent photometric angles (incidence, emission, and phase;  $i$ ,  $e$ , and  $\alpha$ ) are computed using the LOLA 128 pix/deg shape model, the Embree ray-tracing package [4], and the SPICE toolkit [5]. RADF is defined as reflectance relative to a perfectly diffuse (Lambertian) surface illuminated vertically:  $\text{RADF}(i, e, \alpha) = \pi I_0(i, e, \alpha) / (J_0 \times D^2)$ , where  $I_0$  is the observed radiance,  $J_0 = 647 \text{ W/m}^2/\mu\text{m}$  is the solar irradiance at 1064 nm at 1 AU, and  $D$  is the Sun-

Moon distance in AU [6]. The photometric function, derived by dividing RADF by the 1064 nm normal albedo  $A_N$ , contains all illumination and viewing geometry effects [6]. We derive  $A_N$  for every measurement by interpolating the global  $A_N$  map of [7]. The photometric function can be expressed as the product of a disk function  $D(i, e, \alpha)$  that describes the brightness distribution over the lunar disk at a given phase and a phase function  $f(\alpha)$  that describes the drop in radiance as  $\alpha$  increases [6].

**Phase Function:** Presently, we consider two phase functions for fitting to the LOLA data (Figure 1).

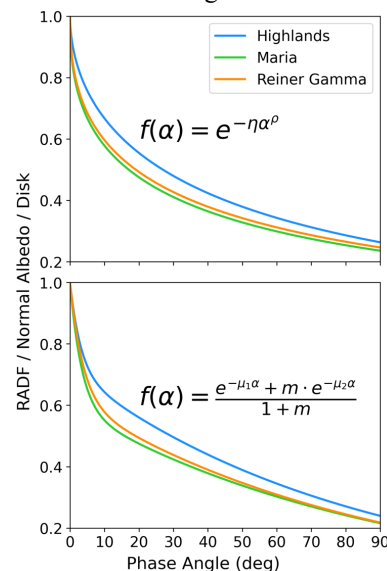


Figure 1: Comparing phase functions for the global highlands and maria with Reiner Gamma. The 2-parameter phase function (top) predicts a shallower decrease at low phase angles than the 3-parameter function, which includes a term for the opposition surge (bottom). Reiner Gamma appears similar to the global maria.

The first is a two-parameter function where  $\eta$  gives the slope and  $\rho$  the “bend” of the phase curve [8].  $\eta$  was found to be inversely correlated with albedo, and  $\rho$  to be correlated with surface roughness. Increased  $\rho$  (i.e., smaller bend) was associated with photometric anomalies caused by high roughness due to factors like boulder fields [8]. The second phase function is a three-parameter function where  $m$  and  $\mu_1$  are associated with the amplitude and width, respectively, of the opposition surge and  $\mu_2$  is correlated with surface roughness [9].

We use the disk function of [10] with both phase functions to fit the global highlands and maria separately, and Figure 1 compares these to the Reiner Gamma swirl albedo anomaly. In these fits, we exclude incidence angles  $> 70^\circ$  to minimize the effects of shadows and errors in the photometric angles, as well as emission angles  $> 60^\circ$  to minimize extreme viewing geometries. For highlands regions where we have sufficient data at low phase angles, the 3-parameter function provides a better fit; however, the 2-parameter function works equally well for maria regions and is more robust to a lack of low-phase-angle data. The importance of low-phase-angle data in constraining the phase function is shown by Figure 2; this need will be addressed by targeted passive radiometry slews for features of interest in support of LRO Extended Science Mission 5. Phase function parameters can be used to adjust observations to a standard viewing geometry [2] to create maps of RADF (Figure 3).

**Future Work:** We will derive global spatially-resolved maps of phase function parameters at  $1^\circ \times 1^\circ$ , applying additional constraints to handle challenges posed by lack of low-phase-angle data. For targets of interest, we will also interpret phase function parameters in terms of geological properties such as iron abundance, optical maturity, and surface roughness. We plan to provide data products of use to the community, such as before-and-after observations of CLPS and Artemis landing sites, and to archive our final passive radiometry data set on the NASA Planetary Data System.

**References:** [1] Ohtake, M. et al. (2013) *Icarus*, 226, 364–374. [2] Yokota, Y. et al. (2011) *Icarus*, 215, 639–660. [3] Barker, M. et al. (2016) 273, 96–113. [4] embree.org [5] naif.jpl.nasa.gov/naif [6] Hapke, B. (2012) Camb. Univ. Press, *Theory of Refl. and Emitt. Spect.*, 2nd ed. [7] Lemelin, M. et al. (2016) *Icarus*, 273, 315–328. [8] Korokhin, V. et al. (2016) *LPSC 47<sup>th</sup>* #1248. [9] Shkuratov, Y. et al. (2011) *PSS* 59, 1326–1371. [10] Akimov, L., et al. (1999) *Kinem. Phys. Celest. Bodies* 15 (4), 232–236.

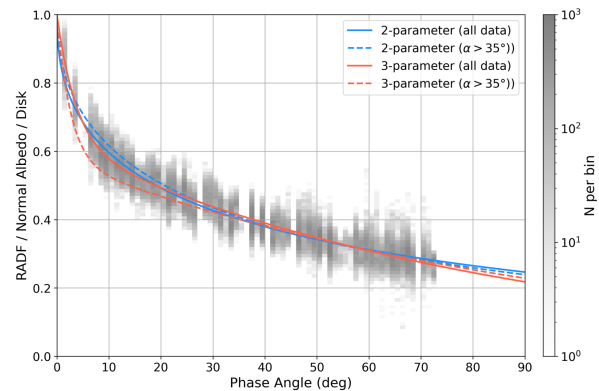


Figure 2: Phase function fits for Reiner Gamma including only data for phase angle  $> 35^\circ$  (dashed lines) are significantly different from those where the full range of phase angles is used (solid lines), demonstrating the importance of observations at low phase angle.

Figure 3: Map of LOLA RADF (16 pix/deg) standardized to  $(i, e, \alpha) = (30^\circ, 0^\circ, 30^\circ)$  using 3-parameter phase function with parameters for maria and highlands from our fits. Light blue areas have no data given the incidence and emission angle cut-offs adopted.

